Aalborg Universitet

AALBORG UNIVERSITY

Using deep learning and meteorological parameters to forecast the photovoltaic generators intra-hour output power interval for smart grid control

Rodríguez, Fermín; Galarza, Ainhoa; Vasquez, Juan C.; Guerrero, Josep M.

Published in:
Energy

DOI (link to publication from Publisher):
10.1016/j.energy.2021.122116

Creative Commons License
CC BY-NC-ND 4.0

Publication date:
2022

Document Version
Publisher's PDF, also known as Version of record

Link to publication from Aalborg University

Citation for published version (APA):
Rodríguez, F., Galarza, A., Vasquez, J. C., & Guerrero, J. M. (2022). Using deep learning and meteorological parameters to forecast the photovoltaic generators intra-hour output power interval for smart grid control. *Energy*, *239*(Part B), Article 122116. https://doi.org/10.1016/j.energy.2021.122116

General rights
Copyright and moral rights for the publications made accessible in the public portal are retained by the authors and/or other copyright owners and it is a condition of accessing publications that users recognise and abide by the legal requirements associated with these rights.

- Users may download and print one copy of any publication from the public portal for the purpose of private study or research.
- You may not further distribute the material or use it for any profit-making activity or commercial gain
- You may freely distribute the URL identifying the publication in the public portal -

Take down policy
If you believe that this document breaches copyright please contact us at vbn@aub.aau.dk providing details, and we will remove access to the work immediately and investigate your claim.

Downloaded from vbn.aau.dk on: December 06, 2025

Energy 239 (2022) 122116

Contents lists available at ScienceDirect

Energy

journal homepage: www.elsevier.com/locate/energy

Using deep learning and meteorological parameters to forecast the photovoltaic generators intra-hour output power interval for smart grid control

Fermín Rodríguez [a, b, *], Ainhoa Galarza [a, b], Juan C. Vasquez [c], Josep M. Guerrero [c]

[a] Ceit-Basque Research and Technology Alliance (BRTA), Manuel Lardizabal 15, 20018, Donostia|San Sebastián, Spain
[b] Universidad de Navarra, Tecnun, Manuel Lardizabal 13, 20018, Donostia/San Sebastián, Spain
[c] Center for Research on Microgrids (CROM), Department of Energy Technology, Aalborg University, Aalborg, 9220, Denmark

ARTICLE INFO

Article history:
Received 9 February 2021
Received in revised form
17 September 2021
Accepted 18 September 2021
Available online 24 September 2021

Keywords:
Confidence interval forecast
Intra-hour horizon
Solar irradiation
Smart control
Photovoltaic generation output power

ABSTRACT

In recent years, the photovoltaic generation installed capacity has been steadily growing thanks to its inexhaustible and non-polluting characteristics. However, solar generators are strongly dependent on intermittent weather parameters, increasing power systems' uncertainty level. Forecasting models have arisen as a feasible solution to decreasing photovoltaic generators' uncertainty level, as they can produce accurate predictions. Traditionally, the vast majority of research studies have focused on the development of accurate prediction point forecasters. However, in recent years some researchers have suggested the concept of prediction interval forecasting, where not only an accurate prediction point but also the confidence level of a given prediction are computed to provide further information. This paper develops a new model for predicting photovoltaic generators' output power confidence interval 10 min ahead, based on deep learning, mathematical probability density functions and meteorological parameters. The model's accuracy has been validated with a real data series collected from Spanish meteorological stations. In addition, two error metrics, prediction interval coverage percentage and Skill score, are computed at a 95% confidence level to examine the model's accuracy. The prediction interval coverage percentage values are greater than the chosen confidence level, which means, as stated in the literature, the proposed model is well-founded.
© 2021 The Author(s). Published by Elsevier Ltd. This is an open access article under the CC BY-NC-ND license (http://creativecommons.org/licenses/by-nc-nd/4.0/).

1. Introduction

Renewable energies have arisen as feasible alternatives to exhaustible fossil energies and a way to reduce greenhouse emissions such as CO_2 and NO_X [1]. For instance, the German government, following European goals for energy transition, has fixed short and long term milestones in order to replace fossil resources with renewable ones. Thus, the share of renewables in the German electric generation matrix must be 20%, 30% and 63% by the end of years 2020, 2025 and 2050, respectively [2]. In order to achieve the stated milestones and support the introduction of renewable generators into the traditional grid, laws were adopted to guarantee renewable plants' profits. Hence, between 2002 and 2017, the installed renewable energy capacity increased 516.67%, i.e. from 18 GW to 111 GW in Germany [3]. This positive trend in installed renewable capacity is also found in other countries, and it is expected to continue in upcoming years [4,5]. However, not all renewable energies have had the same evolution, with solar photovoltaic (PV) and wind technologies being the most widely installed, not only for large scale generators [6] but also in the residential sector, in case of PV generators [7].

Although renewable technologies, and particularly PV generators, are essential for energy transition, it must also be kept in mind that they will be connected to traditional grids. Such networks were linearly structured in that different stakeholders, i.e. generators, transmission system operators, distribution system operators and customers, had well-defined tasks and operating requirements. However, small-scale PV systems are strongly dependent on intermittent, volatile and random meteorological parameters, such as solar irradiation intensity or the cloud effect, making them generators with high levels of uncertainty [8,9]. Large-scale PV

* Corresponding author. Ceit-Basque Research and Technology Alliance (BRTA), Manuel Lardizabal 15, 20018, Donostia\San Sebastián, Spain.
E-mail address: frlalanne@ceit.es (F. Rodríguez).

https://doi.org/10.1016/j.energy.2021.122116
0360-5442/© 2021 The Author(s). Published by Elsevier Ltd. This is an open access article under the CC BY-NC-ND license (http://creativecommons.org/licenses/by-nc-nd/4.0/).

List of abbreviations

Notation	*Description*
ANN	Artificial Neural Network
ARMA	Autoregressive Moving Average
ARIMA	Autoregressive Integrated Moving Average
b_n	Bias value of the n-th neuron
DL	Deep Learning
DPI	Direct Prediction Interval
I	Hidden Neurons
IPI	Indirect Prediction Interval
$J(\widehat{\gamma})$	Jacobian Matrix
L	Recent past deviations
LB_α	Lower Bound for a chosen α
ML	Machine Learning
NPPI	Non-Parametric Prediction Interval
P	Input Parameters
PDF	Probability Distribution Function
PI	Prediction Interval
PICP	Prediction Interval Coverage Percentage
PP	Prediction Point
PPI	Parametric Prediction Interval
PV	Photovoltaic
Gradient vector	
SSN	Skill Score Normalized
STFFNN	Spatiotemporal Feedforward Neural Network
u^2	Unbiased estimator
UB_α	Upper Bound for a chosen α
$w_{p,i}$	Weights of the n-th neuron
x_i	Input vector of the n-th neuron
y	Actual value
$\widehat{y}$	Predicted value
α	Error rate chosen by the user
ε	Approximation error
γ	Set of parameters that model the ANN
γ^*	Optimal set of parameters
$\widehat{\gamma}$	Least squares estimator of ϕ^*
σ^2	Variance

generators are less affected by punctual effects such as clouds movement and have a more stable behaviour. This uncertainty generates unexpected and sudden changes in PV systems' output power, thereby hindering power system operation, and as a result the spread of renewable generators in traditional grids is limited [10]. Therefore, it must be ensured that increasing renewable capacity will not negatively affect power system security and stability in operating conditions [11].

Historically, reversible hydropower plants aside, electric storage devices were not developed for accumulating too much energy. Therefore, electric power systems' decision makers guaranteed grid stability through real-time balancing actions with regard to energy demand and energy generation, along with some energy demand forecasts for different prediction horizons [12,13]. Some of the most relevant tasks that power system decision makers perform are: real-time control, unit commitment or economic dispatch, as well as maintenance scheduling [13,14]. When large and small scale PV generators were introduced into the traditional grid, the uncertainty level of whole power systems increased due to the above explained characteristics of renewable energies. To address this situation, renewable energy generation forecasters emerged as a feasible and effective solution [15].

Due to the wide variety of activities realized by power system decision makers, researchers developed different forecasters, attending to each activity's prediction horizon requirements. In terms of prediction horizon, renewable forecasters are classified into the following main groups [16]:

- **Intra-hour prediction horizon forecasters:** also called nowcasting in the literature [17,18], compute predictions for the desired parameters, going from 1 min to an hour ahead [19]. These forecasters are commonly used in real-time dispatch activities by power system decision makers to keep traditional grids within safe operating requirements [20].
- **Intra-day prediction horizon forecaster:** the literature agrees on fixing a horizon range from one to 6 h ahead [21,22]. Thus, forecast values are used by power system decision makers in intra-day energy markets for load trading proposes in order to ensure grid stability [23].
- **Day-ahead prediction horizon forecasters:** the literature agrees on classifying in this group forecasters whose prediction horizon is between six and 72 h or beyond [24,25]. Forecasters with day-ahead or longer prediction horizons are usually characterized by an hourly resolution to increase the quality of the information provided [26]. Decision makers use the information provided by these forecasters for economic dispatch and unit commitment optimization activities [27,28].

Some studies from the available literature [29–31] state that renewable generators' control strategies must be improved by developing accurate forecasters in all the described prediction horizons, making them more reliable for decision makers. In addition, although up to this moment renewable generators only provide power to the main grid, the European Commission and the International Renewable Energy Agency have started suggesting that renewable generators also provide ancillary services to the main grid [32,33]. Ancillary services can be defined as a set of activities that other stakeholders require from power systems' decision makers in order to keep the traditional grid within stable operating boundary conditions, such as frequency and voltage level boundaries [34]. These services are currently provided by traditional generators due to their relevance to power system operation, as well as their quicker capacity to change to the set up point required by power system decision makers. Therefore, highly accurate intra-hour forecasters will need to be developed in order to allow renewable generators to provide these services [29].

Related to PV energy, the literature agrees that solar irradiation, outdoor temperature and wind speed are the most relevant meteorological parameters involved in power production [35–37]. These parameters not only affect the power PVs generate but also the generators' control parameters such as open voltage circuit, short circuit current and cell temperature [35]. However, of the above listed meteorological parameters, several research studies have demonstrated that solar irradiation has the strongest effect on PV generators' output power [22,35,36]. This is the reason why historically the vast majority of research studies have been focused on predicting the meteorological parameter of solar irradiation for all prediction horizons [3,8,14,19,29,31].

The first solar irradiation forecasters developed to address the

high uncertainty level of PV generators output power were point prediction (PP) forecasters, which were classified as physical or statistical forecasters [38]. Physical forecasters are characterized by the application of weather phenomenon equations [39] and sometimes combined with sky imagery [40] or satellite devices [41], whereas statistical forecasters are based on the combination of historical databases and machine learning (ML) algorithms for regression and feature selection proposes, such as lasso [42,43] algorithms. Physical forecasters are usually less studied due to the expensive equipment and complex mathematical models required. ML statistical forecasters, also noted in the literature as autoregressive models, are based on iterative correlation analyses to fix optimal relationships between forecasters' input and output parameters. Although autoregressive forecasters were acceptable in the first steps in solar irradiation forecasting, their main drawback was their weak capacity to make accurate predictions when commonly unexpected changes occur in solar irradiation values [44–46]. Autoregressive moving average (ARMA) [45] and autoregressive integrated moving average (ARIMA) [46] forecasters are some examples of the first ML forecasters.

To solve the ML forecasters' lack of capacity to predict sudden changes, deep learning (DL) PP forecasters, which are also catalogued as statistical forecasters, arose as a feasible solution. DL forecasters can be either combined with ML to overcome last ones' weakness or constitute as forecasters by themselves [44]. DL forecasters try to emulate through mathematical approximations the human brain's capacity to learn from databases and produce predictions based on previously unseen values [47]. Thus, DL forecasters are commonly referred to as artificial neural networks (ANN) in the literature, and they have been used for various purposes, such as predicting parameters in different research areas [48,49], classification/pattern recognition studies [50] or serving as a baseline for new forecasters to improve forecaster accuracy [51,52].

Although the vast majority of researchers still focus on improving the accuracy PP forecasters, some researchers such as Li et al. [53] and Liu et al. [54] have recently claimed that PP forecasters do not provide complete information because they do not give information about the deviation between actual and forecasted values. In addition, both research studies [53,54] argued that the knowledge of boundaries around forecasted values will provide relevant information to power system decision makers to improve grid stability and operating cost. Thus, prediction interval (PI) forecasters are starting to be developed not only to reduce renewable generator uncertainty [53,55] but also to provide more information related to energy demand forecasting [36].

A literature review on PI forecasters suggests that these forecasters can be classified according to two dimensions. The first dimension examines whether the interval has been calculated through a prediction made by a PP forecaster. Hence, indirect prediction interval (IPI) forecasters use values computed through PP forecasters as a baseline [26,56], whereas direct prediction interval (DPI) forecasters do not use any baseline to compute the interval [55,57]. Although there are few DPI forecasters, recently researchers have examined them more widely. However, the vast majority of researchers still prefer developing accurate PP forecasters in order to develop through them IPI forecasters.

The second dimension examines whether researchers have approximated any parameters of the forecaster through a probability density function (PDF). Forecasters which are based on this PDF approximation are called parametric prediction interval (PPI) forecasters, whereas forecasters that are not based on PDF approximations are known as non-parametric prediction interval (NPPI) forecasters. PPI forecasters usually applied Normal, Gaussian or Laplacian [58,59] PDFs to describe the deviation between actual and forecasted values; these PDFs are then used to compute the interval. However, recent NPPI research studies try to avoid this approximation, arguing that the assumption of describing parameters through single or combined PDFs is speculative, inappropriate and not realistic [3,54,55]. Among all current NPPI forecaster techniques, quantile [54] and bootstrap [60] are the most widely applied ones.

This research paper presents a photovoltaic generator's output power intra-hour PI forecaster through meteorological parameters, specifically for 10 min ahead. Based on the classifications described above, the developed forecaster is catalogued as an indirect parametric PI forecaster. It is indirect because the predicted solar irradiation values obtained through a PP forecaster are used as a baseline to compute the PV generator's output power intervals, and it is parametric because the t-Student PDF has been used to compute the error rate probability chosen by the user. The key contributions of this research study are explained below:

1) A new intra-hour indirect parametric PI forecaster is proposed to estimate PV generator power output 10 min ahead. The developed model combines a DL model, specifically a feedforward spatiotemporal neural network model (used as a baseline model), mathematical theorems and PDFs to compute the interval. The proposed PI forecaster's reliability has been tested with real data series collected from meteorological stations in Vitoria-Gasteiz, Spain.
2) PI forecaster accuracy is commonly studied through reliability and sharpness indexes. Different indexes, namely the prediction interval coverage percentage (PICP) to examine the proposed forecaster's reliability and the Skill score to analyse the computed intervals width, were computed for 95% confidence level under sunny, partially cloudy and cloudy meteorological situations. For the chosen confidence level, with the final fixed forecaster and under the different meteorological situations examined, the computed PICP value is higher than the selected confidence level. The literature agrees [36,59,61] that the PI forecaster model is valid when this situation occurs, and thus the proposed forecaster is considered valid.

2. Methodology

To develop the PI forecaster proposed in this research study, a PP forecaster studied in a previous work is applied as a baseline [62]. Both forecasters i.e. PI and PP forecasters, were developed with same solar irradiation database. Table 1 describes the main characteristics of the PP forecaster, which is based on a DL spatiotemporal feedfordward neural network (STFFNN), whereas Fig. 1 presents the PP forecaster's layout. The STFFNN relies on the combination of a DL feedforward neural network structure and the meteorological databases that contain information from the target and surrounding meteorological stations.

As shown in Fig. 1, DL STFFNN forecasters are ANN structures, which rely on the combination of several parameters that are chosen through sensitivity analyses in order to obtain the best accuracy. Thus, some of the most relevant examined parameters are: the network's layers, each layer's number of neurons, each layer's neuron activation function and learning algorithm.

For the STFFNN PP forecaster used as baseline, the output computed at the hidden layer's i-th neuron is mathematically described as a linear combination of inputs, weights and biases

Table 1
STFFNN PP baseline forecaster's main characteristics.

Input parameters (P)	1168 = season (1), time (1) and solar irradiation data from target (144) and surrounding stations (1022)
Output parameter	solar irradiation
Network structure	Input − hidden − output layers
Hidden Neurons (I)	5
Total amount of Weights (W)	5845
Total amount of Biases (b)	6

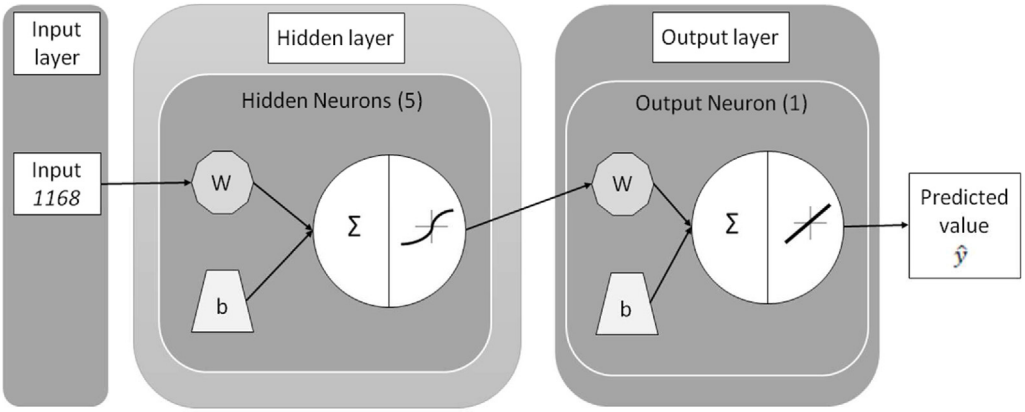

Fig. 1. SPFFNN PP forecaster's layout.

applied in a sigmoidal activation function g:

$$g(x) = \frac{1}{1+e^{-x}} \tag{1}$$

$$x_i = f\left(\sum_{p=1}^{P=1168} [w]_{p,i}[j]_{p,1} + b_i\right) \quad , i \in \{1,2,\ldots,5\} \tag{2}$$

where $j \in \mathbb{R}^{P=1168}$ is the input vector with 1168 dimensions, $w_{p,i}$ refers to i-th neuron's weights with $p \in \{1,2,\ldots,1168\}$, and b_i represents i-th neuron's bias threshold value. In the same way, the output layer's neuron is mathematically described as a linear combination of inputs, i.e. the hidden layer's neuron's output values, weights and biases applied in a linear activation function:

$$\hat{y} = \sum_{i=1}^{I=5} [w_{i,I+1}][g(x_i)] + b_{I+1}. \tag{3}$$

where $\hat{y}$ is not only the output value of the output layer's neuron but also the STFFNN forecaster's predicted point value, which is used as a baseline to build up the PI forecaster.

2.1. Proposed PI methodology

Considering that solar PV generation mainly depends on solar irradiation, let's assume that this meteorological parameter's behaviour (y) can be mathematically expressed as a combination of an unknown scalar function (z) and the parameters involved as

$$y = z(x). \tag{4}$$

Due to the complexity of developing an accurate physical forecaster which describes solar irradiation behaviour (z), the aim is to use the STFFNN PP as an approximation of Eq. (4) in such a way that

$$y = h(x;\gamma^*) + e. \tag{5}$$

Where is defined as the difference between forecasted and actual values and (γ^*) represents the most representative real set (R) of parameters (γ) that better describe solar irradiation behaviour. In addition, selected real (γ^*) parameters can be computed through the Levenberg-Marquardt algorithm, which is based on a least squares problem [63]. Thus, the STFFNN PP forecaster's predicted value $(\hat{y})$ can be expressed as

$$\hat{y} = h(x;\hat{\gamma}). \tag{6}$$

Where $(\hat{\gamma})$ represents the computed (γ^*) parameters computed through the Levenberg-Marquardt algorithm and function (h) is the analytical expression of the STFFNN PP forecaster described in Eq. (3).

Moreover, (e) can also be mathematically described through Taylor's first-order polynomial approximation combined with the two previously defined equations in such way that

$$e = y - h(x;\gamma^*) \approx y - h(x;\hat{\gamma}) - (Q(\hat{\gamma}))^T(\gamma^* - \hat{\gamma}) = y - \hat{y} - (\gamma^* - \hat{\gamma})^T Q(\hat{\gamma}). \tag{7}$$

Where $Q(\hat{\gamma})$ is h's gradient, which is mathematically expressed as

$$Q(\hat{\gamma}) = \left(\frac{\partial h(x;\hat{\gamma})}{\partial \hat{\gamma}_1}, \ldots, \frac{\partial h(x;\hat{\gamma})}{\partial \hat{\gamma}_R}\right)^T \tag{8}$$

Notice that terms in Eq. (7) can be rewritten in such way that

$$y - \hat{y} = e - (\gamma^* - \hat{\gamma})^T Q(\hat{\gamma}). \tag{9}$$

We assume that (y), $(\hat{y})$ and (e) behave as random variables and that (e) follows $N(0,\sigma^2)$ PDF and is independent from $(\gamma^* - \hat{\gamma})$. Hence, Eq. (9) can be mathematically rewritten in root mean square error terms in such way that

$$E\left[(y-\hat{y})^2\right]=E\left[e^2\right]+(Q(\hat{\gamma}))^T E\left[(\hat{\gamma}-\gamma^*)(\hat{\gamma}-\gamma^*)^T\right]Q(\hat{\gamma}). \quad (10)$$

Where E is mathematically defined as expectation and the next property can be used based on the previously explained assumptions,

$$E\left[(\hat{\gamma}-\gamma^*)^T(\hat{\gamma}-\gamma^*)\right]=\sigma^2\left[\mathrm{J}(\hat{\gamma})^T\mathrm{J}(\hat{\gamma})\right]^{-1}. \quad (11)$$

Where $\mathrm{J}_{RxK}(\hat{\gamma})$ is the Jacobian matrix where R is the number of columns in the J matrix whose values are defined by γ^* number of parameters and K is the number of rows in the J matrix whose values are defined by a set of samples of the database used in the forecaster's training step to compute $\hat{\gamma}$. Combining the two equations described above yields the following expression,

$$\begin{aligned} E\left[(y-\hat{y})^2\right] &= \sigma^2\left(1+(Q(\hat{\gamma}))^T\left[\mathrm{J}(\hat{\gamma})^T\mathrm{J}(\hat{\gamma})\right]^{-1}Q(\hat{\gamma})\right) \\ &= \mathrm{u}^2\left(1+(Q(\hat{\gamma}))^T\left[\mathrm{J}(\hat{\gamma})^T\mathrm{J}(\hat{\gamma})\right]^{-1}Q(\hat{\gamma})\right) \\ &= \mathrm{u}^2\left(1+(Q(\hat{\gamma}))^T D^{-1}Q(\hat{\gamma})\right) \end{aligned} \quad (12)$$

where u^2 is defined as the σ^2 parameter's unbiased estimator, whose value is defined as,

$$u^2=\frac{1}{K-R}\sum_{k=1}^{K}(y_k-h(x_k;\hat{\gamma}))^2. \quad (13)$$

Observe that the unbiased estimator parameter, u^2, can just be computed if $K>R$; otherwise, the forecaster will not predict the interval properly. This condition must also be taken into account when the J matrix's dimensions are chosen. Finally, for sufficient number of K samples from the training database used to develop the baseline model, the random parameter T can be mathematically defined in such way that

$$T=\frac{y-\hat{y}}{u\sqrt{1+(Q(\hat{\gamma}))^T D^{-1}Q(\hat{\gamma})}} \quad (14)$$

and whose behavior can be described by a Student's t-distribution PDF with $K-R$ degrees of freedom [64]. Thus, the PI for estimation $\hat{y}$ obtained through the PP forecaster with confidence $100(1-\alpha)\%$ is computed by

$$\mathrm{PI}=\hat{y}\pm t_{R-K}^{\alpha/2}u\sqrt{1+(Q(\hat{\gamma}))^T D^{-1}Q(\hat{\gamma})}. \quad (15)$$

Where $\alpha\in[0,1]$ represent the user's selected error rate, $t_{R-K}^{\alpha/2}=P\left(T<\frac{\alpha}{2}\right)$ and P refers to probability.

2.2. Benchmark model

To compare the results obtained by proposed PI forecaster in the above section, the methodology proposed by Yan et al. [65] with some modification has been computed as benchmark. In Ref. [65], Yan et al. proposed to compute the interval forecasting based on recent deviations between actual and forecasted values combined with an ANN to predict future deviations. In a second step, future deviations are approximated through a Normal PDF to compute the intervals. Attending to the two criterion explained in Section 1, Yan et al.'s methodology can be classified as indirect and parametric PI forecaster; indirect because it applies a PP forecaster to compute the interval and parametric because Yan et al. approximated future deviations between actual and predicted values through a Normal PDF. Therefore, in Yan et al.'s forecaster two parameters need to be selected: the error rate chosen by the end user α and the number of recent past deviations (L) that will be taken into account for computing the intervals. In this study, Yan et al. forecaster's second step was omitted, and the Normal PDF approximation was directly done with previous deviations. Fig. 2 shows a layout about how computed benchmark model works.

2.3. PI forecasters error metrics

A literature review on PI forecaster accuracy error metrics suggests that these indexes are catalogued in two dimensions, reliability and sharpness metrics [26,36,53,58]. Reliability metrics examine PI forecasters' accuracy, i.e., how many of the actual values fall into forecasted intervals. Among all reliability metrics, prediction interval coverage percentage (PICP) is the most widely computed error metric [54,66]. Sharpness metrics analyse predicted interval width, i.e., how close predicted interval's bounds are. In this study, a Skill score (SS) is computed to examine the proposed forecaster's sharpness.

By combining equations (6) and (15), the PI's lower bound (LB) and upper bound (UB) for a time instance m, y_m can be expressed in such way that,

$$\mathrm{LB}_\alpha(x_m)=h(x_m;\hat{\gamma})-t_{R-K}^{\alpha/2}u\sqrt{1+(Q(\hat{\gamma}))^T D^{-1}Q(\hat{\gamma})}, \quad (16)$$

$$\mathrm{UB}_\alpha(x_m)=h(x_m;\hat{\gamma})+t_{R-K}^{\alpha/2}u\sqrt{1+(Q(\hat{\gamma}))^T D^{-1}Q(\hat{\gamma})}. \quad (17)$$

Once the PI's bounds are mathematically defined, PICP can be described as,

$$PICP_\alpha=\frac{1}{M}\sum_{m=1}^{M}\delta_m^\alpha \quad \delta_m^\alpha=\begin{cases}1, & y_m\in PI_m^\alpha\\ 0, & y_m\notin PI_m^\alpha\end{cases}. \quad (18)$$

Where δ_m^α is a Boolean parameter which takes the value 1 if the actual value y_m falls into the forecasted interval and the value 0 if it does not. M represents the number of samples examined. Moreover, the condition $PICP_\alpha>1-\alpha$ must be met to consider the proposed PI forecaster as being suitable [54,66], otherwise the proposed forecaster needs to be examined until this condition is met; $1-\alpha$ value is also known as confidence level CL_α.

To examine the predicted intervals for M actual values, the SS error metric can be computed in such way that

$$SS_\alpha=\frac{1}{M}\sum_{m=1}^{M}|\delta_m^\alpha-(1-\alpha)|\max(|LB_\alpha(x_m)-y_m|,|y_m-UB_\alpha(x_m)|) \quad (19)$$

Eq. (19) demonstrates that in the SS_α metric, the actual values y_m that fall into the PI have a lower penalty than when y_m values fall out. In addition, SS_α must always be positive and the closest the SS_α value is from zero, the better sharpness the PI has. Usually, the SS_α value is normalized through parameter N to make facilitate comparison with other research studies in the literature,

$$SSN_\alpha=\frac{1}{N}SS_\alpha. \quad (20)$$

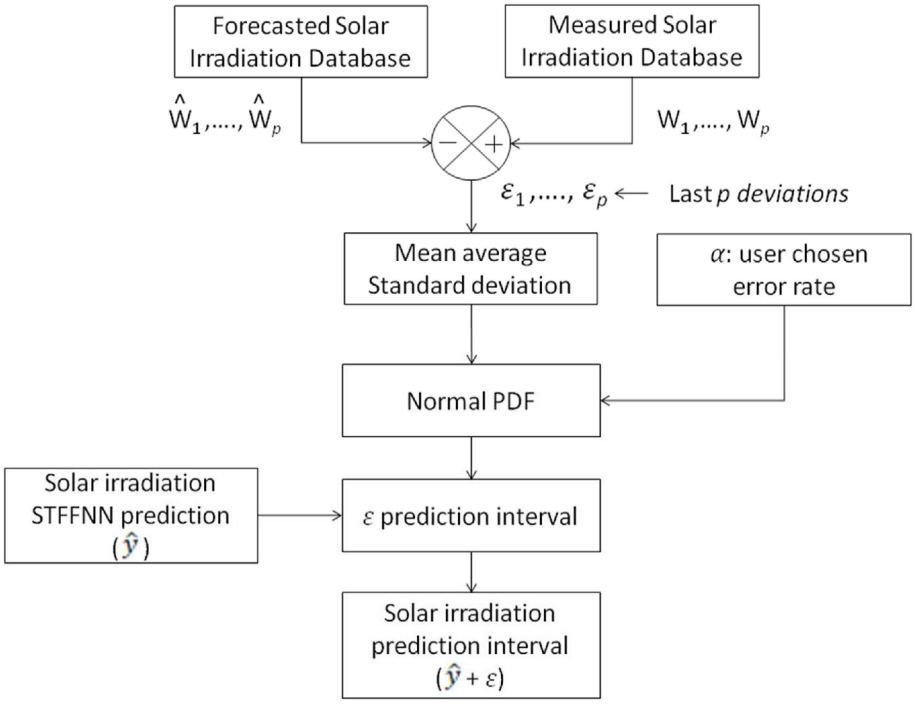

Fig. 2. Benchmark PI forecaster's layout.

3. Results

In this section, the proposed DL PI forecaster's accuracy is examined. Our model predicts photovoltaic generators' output power interval through meteorological parameters, specifically through solar irradiation, for 10 min ahead. In order to make a real assessment, a solar irradiation database provided by Euskalmet, the Basque Government's Meteorological Agency (http://www.euskalmet.euskadi.eus/), is used. The selected solar irradiation database has 10 min resolution and had to be the same as the one used in the development of STFFNN forecaster. While the whole database for years 2015–16 was used in the STFFNN forecaster's training step, the entire database for year 2017 was used in the STFFNN forecaster's validation [62]. Thus, in this study it was also mandatory to use same databases, but for different purposes; the 2015-16 database was applied to compute the Jacobian matrix $J(\hat{\gamma})$, whereas the 2017 database was applied to calculate the gradient vector $Q(\hat{\gamma})$ in ('C040 Vitoria-Gasteiz, Spain'). Attending to Köppen-Geiger climate classification, Vitoria-Gasteiz, Spain has an oceanic climate, but at the same time is 60 km inland with yearly average temperature and precipitations of 11.4 °C and 782.3 mm, respectively.

3.1. Results of proposed solar irradiation PI forecaster

As explained above, the $J(\hat{\gamma})$ matrix has R x K dimension and the condition $K > R$ must be satisfied to properly compute the u^2 estimator (see Eq. (13)). Therefore, it is mandatory to first calculate R parameter, which represents the set of parameters that describe the STFFNN PP forecaster. Parameter R can be computed in such a way that

$$R = Ix(P+2)+1 = W+b = 5851. \quad (21)$$

The second step consists of computing dimension K for matrix $J(\hat{\gamma})$ in such a way that the proposed PI forecaster's accuracy is maximized for solar irradiation forecasting 10 min ahead. For this purpose, a sensitivity analysis was run, where in order to consider the proposed PI forecaster acceptable, parameter K is varied until the condition $PICP_\alpha > (1-\alpha)$ is achieved. Thus, dimension K of the $J(\hat{\gamma})$ matrix must satisfy the following condition, $105264 > K > R = 5851$ where 105264 is the length of the training database used to develop the PP baseline forecaster. Moreover, remember that, for the proposed algorithm for each examined K set, parameters described in Eqs. (13)–(15) need to be calculated. To better examine the proposed solar irradiation PI forecaster, whole 2017 year was analysed, consisting of 72 sunny days, 47 partially cloudy days and 246 cloudy days whose results are reported in Table 2. Noted that for each K set different analyses were done; while "Global" makes reference to the error metrics for whole days of 2017, there are also provided same error metric by each type of day, i.e. sunny, partially cloudy or cloudy. Concerning the error metrics presented in Table 2, $\%_{(PICP>95)}$, gives in % for each set of data the number of days that satisfied the condition $PICP > 0.95$, then for those days that satisfied the condition, $\overline{PICP}$, σ_{PICP}, $PICP_{MAX}$ and $PICP_{MIN}$ indicate the mean average, the standard deviation and the maximum and minimum values, respectively. $M = 144$ represents the number of predicted values during each day.

The results in Table 2 demonstrate that no matter which type of day is being analysed (sunny, partially cloudy or cloudy), the lower dimension K is, the higher the $PICP_\alpha$ value is. This fact is related to DL overfitting phenomena, which is based on the fact that if too much similar data is used, the forecaster is not able to learn and instead memorizes values, reducing its generalization capacity.

However, it can also be seen in Table 2 how there are some accuracy differences depending on the type of day examined. For instance, for $K = 5974$ and sunny days, 95.77% fulfil the condition $PICP_\alpha > (1-\alpha)$, whereas for the same K dimension and cloudy days, only 38.26% of the days fulfil the condition. In addition, it is also necessary to examine the sharpness of the predicted intervals.

Table 2
$PICP_{0.05}$ results for solar irradiation PI forecasting.

Error metric	K	Analysis	$\%_{(PICP>95)}$	$\overline{PICP}$	σ_{PICP}	$PICP_{MAX}$	$PICP_{MIN}$
100 × PICP (M = 144)	6000	Global	43.48	97.54	1.52	100.00	95.14
		Sunny	95.77	98.35	1.33	100.00	95.14
		Partially Cloudy	77.27	97.06	1.22	99.31	95.14
		Cloudy	20.87	96.85	1.52	100.00	95.14
	5974	Global	55.07	97.71	1.57	100.00	95.14
		Sunny	95.77	98.58	1.44	100.00	95.14
		Partially Cloudy	77.27	97.66	1.25	100.00	95.83
		Cloudy	38.26	97.91	1.46	100.00	95.14
	5953	Global	73.33	97.88	1.58	100.00	95.14
		Sunny	98.59	99.09	1.10	100.00	95.14
		Partially Cloudy	90.91	98.09	1.33	100.00	95.14
		Cloudy	62.17	97.22	1.47	100.00	95.14
	5943	Global	82.32	98.19	1.49	100.00	95.14
		Sunny	100.00	99.39	0.97	100.00	95.14
		Partially Cloudy	100.00	98.20	1.44	100.00	95.14
		Cloudy	73.48	97.67	1.39	100.00	95.14
	5937	Global	85.22	98.25	1.54	100.00	95.14
		Sunny	100.00	99.47	0.88	100.00	95.14
		Partially Cloudy	100.00	98.45	1.41	100.00	95.14
		Cloudy	77.83	97.79	1.45	100.00	95.14

Table 3
$SSN_{0.05}$ results for solar irradiation PI forecasting for sunny days.

Error metric	K	Analysis	$\overline{SSN}$	σ_{SSN}	SSN_{MAX}	SSN_{MIN}
100 × SSN (M = 144)	6000	Global	2.29	1.70	7.93	0.45
		Sunny	1.28	0.64	2.98	0.45
		Partially Cloudy	2.09	1.04	4.00	0.70
		Cloudy	3.53	2.00	7.93	0.70
	5974	Global	2.86	2.14	11.23	0.51
		Sunny	1.43	0.73	3.53	0.51
		Partially Cloudy	2.27	1.12	4.78	0.73
		Cloudy	4.16	2.14	11.23	0.79
	5953	Global	3.36	2.33	11.13	0.58
		Sunny	1.63	0.87	4.22	0.58
		Partially Cloudy	2.50	1.34	6.20	0.86
		Cloudy	4.44	2.43	11.13	0.67
	5943	Global	3.66	2.47	11.60	0.63
		Sunny	1.80	0.98	4.83	0.63
		Partially Cloudy	2.67	1.50	6.51	0.97
		Cloudy	4.70	2.54	11.60	0.63
	5937	Global	3.74	2.50	11.27	0.63
		Sunny	1.88	1.04	5.10	0.66
		Partially Cloudy	2.74	1.58	6.92	0.98
		Cloudy	4.71	2.58	11.27	0.63

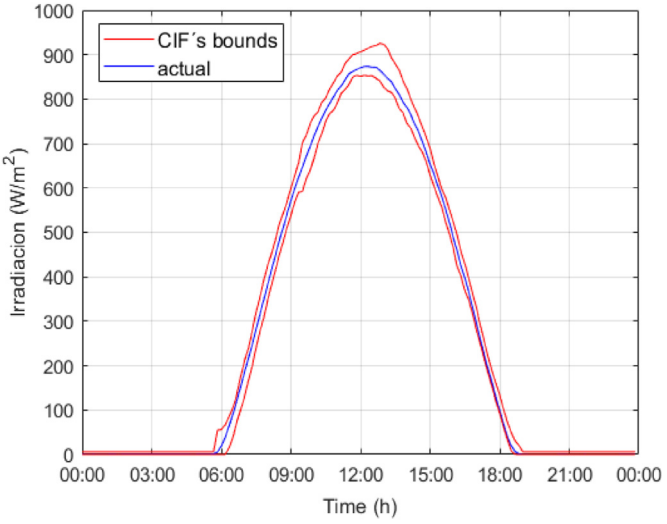

Fig. 3. Forecasted intervals and actual solar irradiation evolution for April 8, 2017 (sunny day, $PICP_{0.05} = 100$ and $SSN_{0.05} = 0.69$).

Table 3 shows the $SSN_{0.05}$ error metrics results for sunny, partially cloudy and cloudy days. In addition, it must be taken into account that the N value for normalizing the $SSN_{0.05}$ value is computed as the average of solar irradiation per day per year, 158.02 W/m^2. For those days that satisfied the condition $PICP_\alpha > (1 - \alpha)$, $\overline{SSN}$, σ_{SSN}, SSN_{MAX} and SSN_{MIN} indicate the mean average, the standard deviation and the maximum and minimum values. $M = 144$ represents the number of predicted values during each day.

After examining the results of Table 2, it is concluded that the lower the K parameter is, the higher the $SSN_{0.05}$ index. Therefore, if results of sunny, partially cloudy and cloudy days are simultaneously examined, it can be observed that there is a relationship between interval width and forecasters accuracy, and thus the reliability ($PICP_{0.05}$) and sharpness ($SSN_{0.05}$) indexes must be balanced. Although in this study we have chosen $K = 5937$, this parameter, as well as α error metric, can be modified by the end user. Figs. 3–5 show the forecasted solar irradiation intervals for a sunny, partially cloudy and cloud day, respectively.

3.2. Results of computed solar irradiation PI benchmark forecaster

As explained above, in computed benchmark two parameters need to be selected: the error rate chosen by the end user α and the number of recent past deviations L that will be taken into account for computing the intervals. Predictions in the above section were done with $\alpha = 0.05$ so, this value will be the same to ensure a proper comparison between both methods. Therefore, L is the only parameter that must be selected. For this purpose, a sensitivity analysis was run, where in order to consider the computed benchmark acceptable, parameter L is varied until the condition $PICP_\alpha > (1 - \alpha)$ is met. Same criteria followed in above section to construct Tables 2 and 3 has been used to construct Tables 4 and 5 that summarizes the results of the benchmark model.

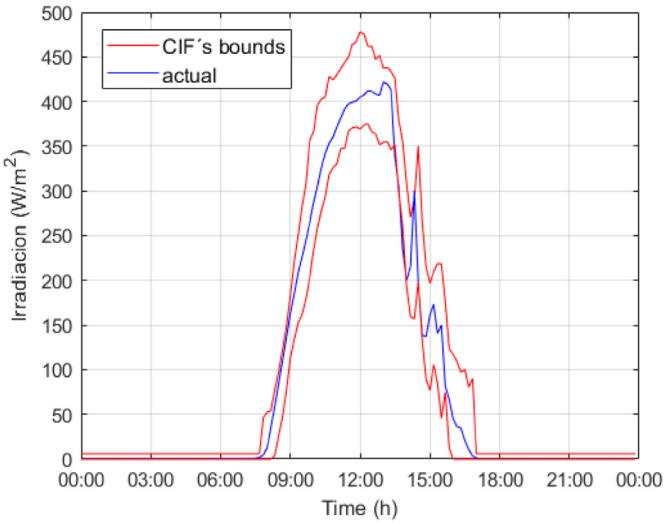

Fig. 4. Forecasted intervals and actual solar irradiation evolution for January 4, 2017 (partially cloudy day,$PICP_{0.05} = 97.22$ and $SSN_{0.05} = 1.07$).

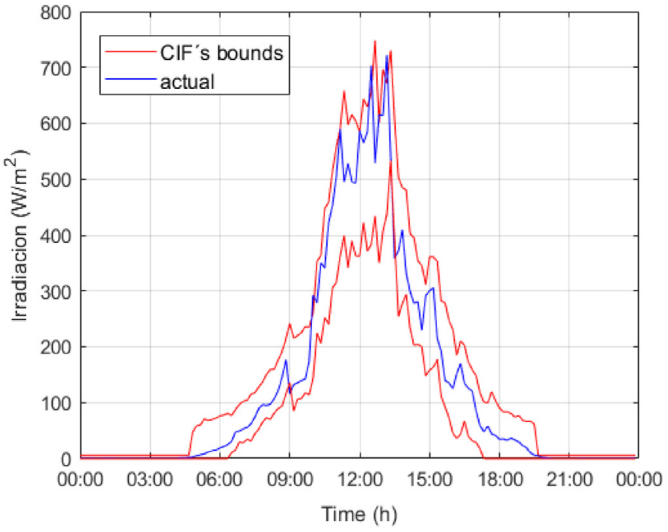

Fig. 5. Forecasted intervals and actual solar irradiation evolution for June 15, 2017 (cloudy day, $PICP_{0.05} = 95.83$ and $SSN_{0.05} = 2.56$).

After examining the results of Tables 4 and 5, it is concluded that only when the last two recent deviations, $L = 2$, are taken into account to forecast the intervals, the computed benchmark works. Figs. 6–8 show the forecasted solar irradiation intervals for same sunny, partially cloudy and cloud day presented in Figs. 3–5.

3.3. Comparison between proposed and benchmark models

In order to ensure a proper comparison between both methods remind that the predictions of both forecasters were computed for the same error rate, $\alpha = 0.05$. While proposed PI forecaster's best accuracy is obtained for $K = 5937$, computed PI benchmark's best accuracy is obtained for $L = 2$. To make it easier the comparison between both methods, Tables 6 and 7 summarizes the results of both methods. While Table 6 summarizes $PICP_{0.05}$ results, Table 7 summarizes $SSN_{0.05}$ results. In addition, to make a deeper comparison among two methods in Table 6 the error metrics were also computed for those days that did not satisfied the conditionPICP > 95. Concerning to Table 7, error metric $SSN_{0.05}$ was only computed for those cases were the condition PICP > 95 was satisfied.

Based on the results presented in Table 6, it can be concluded that proposed methodology has better accuracy in every analysis due to the fact that the $\%_{(PICP>95)}$ is higher in this methodology than in the benchmark. In addition, in the vast majority of the computed metrics the proposed methodology obtained better results than the benchmark. The only case where the benchmark model obtains better results than proposed model is in "Cloudy" analysis for the $PICP_{MIN}$ error metric. Concerning the results summarized in Table 7, it is shown that the proposed model performs better than benchmark model owing to the fact that the proposed model produces narrower intervals. Therefore, this model has been used to compute PV generators output power in the following section.

3.4. Results of PI for photovoltaic generator output power

Once the solar irradiation DL PI forecaster's accuracy has been examined, the forecasted solar irradiation interval values (see Eqs. (16) and (17)) and a mathematical expression that describes the solar PV's output power production [36,47] are combined to calculate a PV power generation interval,

$$PVPLB_{\alpha}(x_m) = \eta * A * SILB_{\alpha}(x_m) * (1 - 0.005 * (C_m - 25)). \quad (22)$$

$$PVPUB_{\alpha}(x_m) = \eta * A * SIUB_{\alpha}(x_m) * (1 - 0.005 * (C_m - 25)). \quad (23)$$

Where $PVPLB_{\alpha}(x_m)$ and $PVPUB_{\alpha}(x_m)$ represent the lower and upper interval bounds of the PV generators' output power at m instance for the user's chosen α error rate, respectively; η is defined as the generator's conversion efficiency rate; A represents the surface of the PV (m^2); $SILB_{\alpha}(x_m)$ and $SIUB_{\alpha}(x_m)$ represent the solar irradiation lower and upper interval bounds obtained through the developed DL STFFNN PI forecaster at m instance for the user's chosen α error rate, respectively; and C_m is the ambient temperature in (°C). To be able to calculate power generated, a commercial panel with the following characteristics was selected: $\eta = 17.59\%$ and $S = 1.6767\ m^2$. Table 8 shows the computed $PICP_{0.05}$ and $SSN_{0.05}$ indexes with $K = 5937$ for the PV generator's output power on sunny, partially cloudy and cloudy days.

The results in Table 8 show that the developed PI forecaster is able to predict with sufficient accuracy the examined PV generator's output power under different meteorological conditions (sunny, partially cloudy and cloudy days) for error rate. As is the case for solar irradiation PI forecasters, indexes for sunny meteorological conditions are better than for partially cloudy and cloudy conditions, so it can be concluded that when there are fewer sudden changes the proposed PI forecaster has higher reliability. In addition, Figs. 9–11 show the forecasted PV generator's output power intervals for the solar irradiation on sunny, partially cloudy and cloud days examined in Figs. 3–5.

Once the PV output power PI STFFNN forecaster's architecture has been fixed, and its reliability has been examined under different meteorological conditions, the next step consists of examining similar research studies [54,67] available in the literature and comparing published results against those computed by the proposed PI STFFNN forecaster.

Pedro et al. [67] examined the accuracy of analysing different DL

Table 4
$PICP_{0.05}$ results for solar irradiation PI benchmark forecasting.

Error metric	L	Analysis	$\%_{(PICP>95)}$	$\overline{PICP}$	σ_{PICP}	$PICP_{MAX}$	$PICP_{MIN}$
100 × PICP (M = 144)	144	Global	0.00	0.00	0.00	0.00	0.00
		Sunny	0.00	0.00	0.00	0.00	0.00
		Partially Cloudy	0.00	0.00	0.00	0.00	0.00
		Cloudy	0.00	0.00	0.00	0.00	0.00
	36	Global	0.00	0.00	0.00	0.00	0.00
		Sunny	0.00	0.00	0.00	0.00	0.00
		Partially Cloudy	0.00	0.00	0.00	0.00	0.00
		Cloudy	0.00	0.00	0.00	0.00	0.00
	6	Global	0.00	0.00	0.00	0.00	0.00
		Sunny	0.00	0.00	0.00	0.00	0.00
		Partially Cloudy	0.00	0.00	0.00	0.00	0.00
		Cloudy	0.00	0.00	0.00	0.00	0.00
	3	Global	0.00	0.00	0.00	0.00	0.00
		Sunny	0.00	0.00	0.00	0.00	0.00
		Partially Cloudy	0.00	0.00	0.00	0.00	0.00
		Cloudy	0.00	0.00	0.00	0.00	0.00
	2	Global	68.41	96.33	0.96	98.61	95.14
		Sunny	67.61	96.24	0.93	98.61	95.14
		Partially Cloudy	68.18	96.04	0.86	97.92	95.14
		Cloudy	68.70	96.42	0.97	98.61	95.14

Table 5
$SSN_{0.05}$ results for solar irradiation PI benchmark forecasting.

Error metric	L	Analysis	$\overline{SSN}$	σ_{SSN}	SSN_{MAX}	SSN_{MIN}
100 × SSN (M = 144)	2	Global	10.18	8.84	42.27	0.70
		Sunny	2.24	1.46	7.92	0.70
		Partially Cloudy	6.24	3.43	17.67	1.59
		Cloudy	13.50	9.06	42.27	0.70

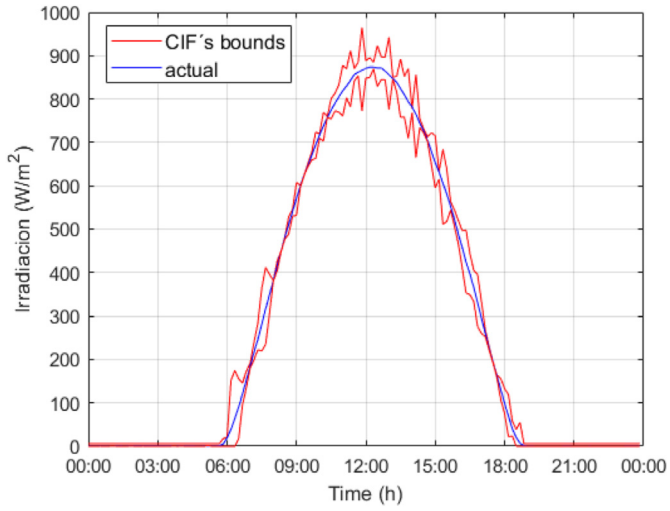

Fig. 6. Forecasted intervals and actual solar irradiation evolution for April 8, 2017 (sunny day, $PICP_{0.05} = 96.53$ and $SSN_{0.05} = 0.75$).

methods such as k-nearest-neighbours and gradient-boosting and combining them with quantile generation techniques to predict solar irradiation intervals for different intra-hour prediction horizons. Pedro et al.'s proposed PI forecaster also took as baseline the value produced by a PP forecaster that used solar irradiation data as well as sky-imagery to produce the point prediction value. After the point value has been computed, the probabilistic quantile generation technique is applied to compute the prediction interval. Note that each DL PP forecaster examined in Ref. [67] has its own way of computing the quantiles to predict the intervals based on the fact that each method has its own characteristics. For the 10-min-ahead

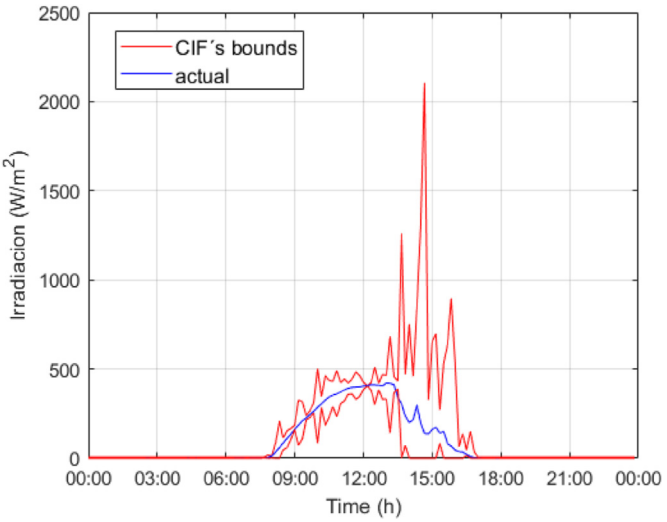

Fig. 7. Forecasted intervals and actual solar irradiation evolution for January 4, 2017 (partially cloudy day, $PICP_{0.05} = 95.14$ and $SSN_{0.05} = 2.96$).

prediction horizon, Pedro et al. obtained PICP indexes whose accuracy were between 39.8% and 84.7%. In that study, Pedro et al. did not differentiate between sunny, partially cloudy and cloudy days, which makes it more difficult to compare both studies. However, based on the fact that our solar irradiation PI forecaster has accuracy greater than 95%, it seems that ours could slightly improve the PI forecaster proposed in Ref. [67].

Liu et al. [54] combined generalized regression, extreme machine learning and Elman neural networks through the use of genetic and back-propagation learning algorithms to compute a weight-varying combination forecast mode PP forecaster. Then, the point values obtained by their proposed model are used as a baseline and combined with a nonparametric kernel density estimation, which takes into account the statistical distribution of the PP forecaster's errors to predict the PV generator's output power interval for 5 min ahead. In this case, Liu et al. classified days into: rainy, partially cloud, cloudy and sunny weather conditions, obtaining 95.05%, 95.62%, 96.05% and 97.08% $PICP_{0.05}$ values, respectively. Our PI PV generator's output power forecaster for

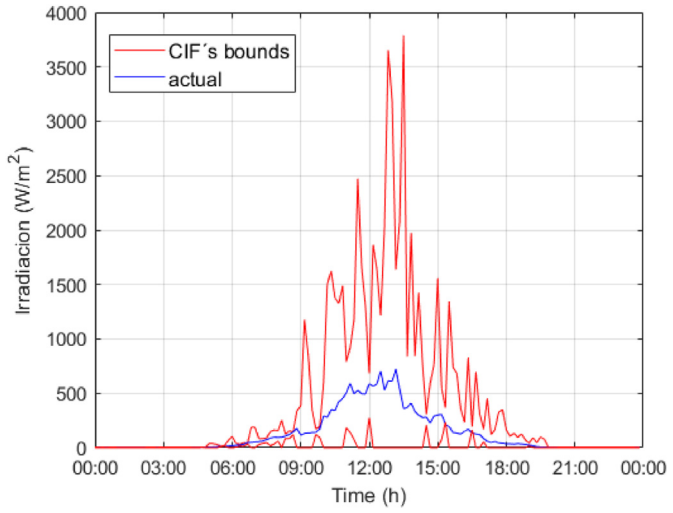

Fig. 8. Forecasted intervals and actual solar irradiation evolution for June 15, 2017 (cloudy day, $PICP_{0.05} = 95.83$ and $SSN_{0.05} = 4.15$).

10 min ahead under sunny, partially cloudy and cloudy days has obtained 99.47%, 98.45% and 97.78% averaged $PICP_{0.05}$ values. Therefore, it can be demonstrated how our forecaster slightly improves Liu et al.'s under partially cloud, cloudy and sunny meteorological conditions.

4. Conclusions

This research study proposes an indirect parametric PI PV generator's output power for 10 min ahead using meteorological parameter information. These are the conclusions from this study:

1) The developed model combines a DL model, specifically a feedforward spatiotemporal neural network model that is used as a baseline model, mathematical theorems and a t-Student PDF to compute the interval. In addition, the forecaster predicts the interval based on the error rate chosen by the end user, and the developed forecaster's reliability and interval width was examined by using a real solar irradiation database from Vitoria-Gasteiz, Spain and different error metrics.

Table 6
$PICP_{0.05}$ results comparison between proposed and benchmark models for solar irradiation PI forecasting.

Model	Analysis	$\%_{(PICP>95)}$	$\%_{(PICP<95)}$	$\overline{PICP}$	σ_{PICP}	$PICP_{MAX}$	$PICP_{MIN}$
Proposed	Global	85.22	–	98.25	1.54	100.00	95.14
		–	14.78	92.06	1.77	94.44	86.81
	Sunny	100.00	–	99.47	0.88	100.00	95.14
		–	0.00	–	–	–	–
	Partially Cloudy	100.00	–	98.45	1.41	100.00	95.14
		–	0.00	–	–	–	–
	Cloudy	77.83	–	97.79	1.45	100.00	95.14
		–	22.17	92.09	1.77	94.44	86.81
Benchmark	Global	68.41	–	96.33	0.96	98.61	95.14
		–	31.59	93.48	1.03	94.44	90.28
	Sunny	67.61	–	96.24	0.93	98.61	95.14
		–	32.39	93.45	0.89	94.44	90.97
	Partially Cloudy	68.18	–	96.04	0.86	97.92	95.14
		–	31.82	93.86	0.85	94.44	90.36
	Cloudy	68.70	–	96.42	0.97	98.61	95.14
		–	31.30	93.41	1.08	94.44	90.28

Table 7
$SSN_{0.05}$ results comparison between proposed and benchmark models for solar irradiation PI forecasting.

Model	Analysis	$\overline{SSN}$	σ_{SSN}	SSN_{MAX}	SSN_{MIN}
Proposed	Global	3.74	2.50	11.27	0.63
	Sunny	1.88	1.04	5.10	0.66
	Partially Cloudy	2.74	1.58	6.92	0.98
	Cloudy	4.71	2.58	11.27	0.63
Benchmark	Global	10.18	8.84	42.27	0.70
	Sunny	2.24	1.46	7.92	0.70
	Partially Cloudy	6.24	3.43	17.67	1.59
	Cloudy	13.50	9.06	42.27	0.70

Table 8
$SSN_{0.05}$ and $PICP_{0.05}$ results for the predicted PV generator's output power.

Analysis	$\%_{(PICP>95)}$	$\overline{PICP}$	σ_{PICP}	$\overline{SSN}$	σ_{SSN}
Global	84.93	98.25	1.54	1.16	0.81
Sunny	100.00	99.47	0.88	0.57	0.31
Partially Cloudy	100.00	98.45	1.41	0.84	0.47
Cloudy	77.39	97.78	1.45	1.47	0.85

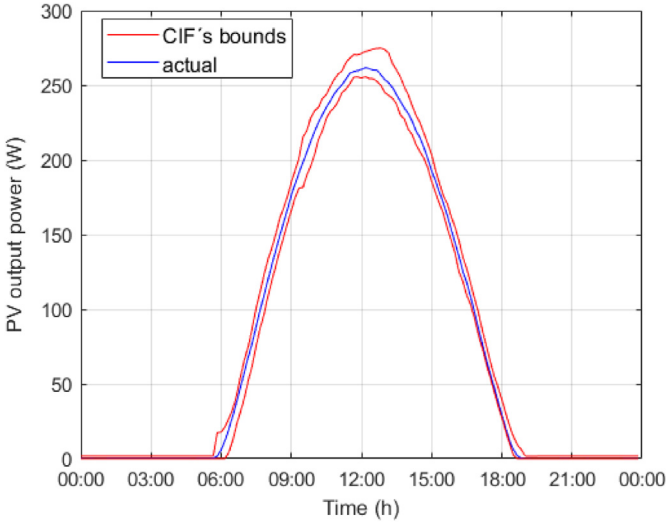

Fig. 9. Forecasted intervals and actual PV generator's output power evolution for April 8, 2017 (sunny day, $PICP_{0.05} = 100.00$ and $SSN_{0.05} = 0.23$).

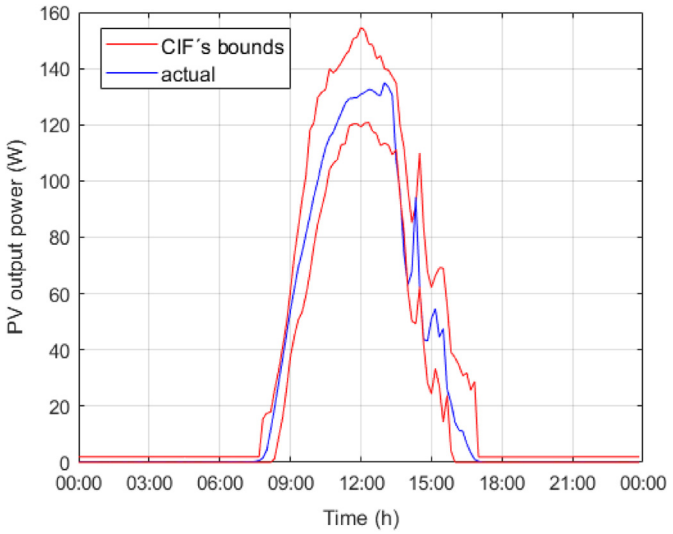

Fig. 10. Forecasted intervals and actual PV generator's output power evolution for January 4, 2017 (partially cloudy day, $PICP_{0.05} = 97.22$ and $SSN_{0.05} = 0.35$).

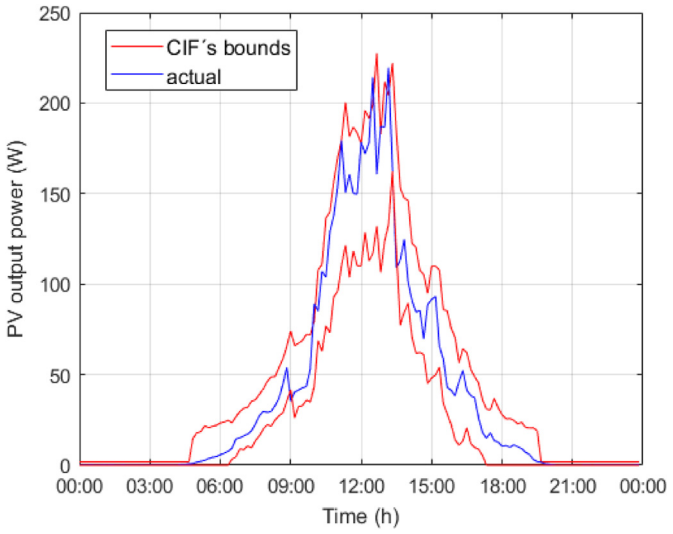

Fig. 11. Forecasted intervals and actual PV generator's output power evolution for June 15, 2017 (cloudy day, $PICP_{0.05} = 95.14$ and $SSN_{0.05} = 0.78$).

2) The solar irradiation PI forecaster has been validated with the entire data of 2017. Attending to the accuracy results shown in Table 6, proposed forecaster satisfied required condition of $PICP_{0.05} > 0.95$ in the 85.22% days of 2017. While for those days which met the condition $\overline{PICP_{0.05}}$ is 98.25, the $\overline{PICP_{0.05}}$ value for those days that did not meet the condition is 92.06. If these error metrics results are contrasted against those provided by computed benchmark, only the 68.41% of the days of 2017 met the condition of $PICP_{0.05} > 0.95$. While for those days which met the condition $\overline{PICP_{0.05}}$ is 96.33, the $\overline{PICP_{0.05}}$ value for those days that did not meet the condition is 93.48. Therefore, it was demonstrated that proposed forecaster performs better than computed benchmark PI forecaster. The reason why $\overline{PICP_{0.05}}$ values is higher in the benchmark model than in proposed one for those days that did not meet the condition, relies on the fact that is that there were some days close to meet the condition. Therefore, the value of the $\overline{PICP_{0.05}}$ error metric rises up in the benchmark model.
3) Attending to the sharpness error metrics results shown in Table 7, for those days where the condition $PICP_{0.05} > 0.95$ was met, proposed prediction model obtained a $\overline{SSN_{0.05}}$ error metric of 3.74, whereas computed benchmark model got 10.18. This error metric was computed for each subset data of sunny, partially cloudy and cloudy days; while the obtained $\overline{SSN_{0.05}}$ for proposed model is 1.88, 2.74 and 4.71, respectively, for computed benchmark is 2.24, 6.24 and 13.50. Therefore, it is concluded that proposed forecaster does not only have higher accuracy, but also produces narrower intervals.
4) Through the predictions done by proposed solar irradiation PI forecaster, PV output power generator's intervals were computed. For entire 2017 year's data, the 84.93% of computed days satisfied the condition $PICP_{0.05} > 0.95$, with a global $\overline{PICP}$ of 98.25 and $\overline{SSN}$ of 1.16. If each type of days subsets are examined sunny and partially cloudy days obtained remarkable results sue to the fact that in both cases the 100.00% of computed days satisfied the condition $PICP_{0.05} > 0.95$, this value reduces to the 77.39% in cloudy days. $\overline{PICP}$ and $\overline{SSN}$ error metrics were computed for each subset data of sunny, partially cloudy and cloudy days; while the obtained $\overline{PICP}$ for proposed model are 99.47, 98.45 and 97.78, respectively, for $\overline{SSN}$are 0.57, 0.84 and 1.47. Therefore, developed forecaster makes it possible to provide further information to power systems' decision makers, doing possible in near future not only to provide power generation but also ancillary services, maximizing PV generators' profits
5) The computed numerical results of this research activity and the sensitivity analyses were done using meteorological data from the location of Vitoria-Gasteiz, Spain. While the database for the years 2015–16 was applied for computing $J(\hat{\gamma})$, the 2017 database was applied to calculate $Q(\hat{\gamma})$. Therefore, the examined mathematical methodology for PV generator output power PI forecasting can be easily applied in other locations. However, the biggest disadvantage of the present methodology is the need to have a database from the target station to fit the model's parameters.

Credit author statement

Fermín Rodríguez: Conceptualization, Methodology, Validation, Resources, Investigation, Writing – original draft, Ainhoa Galarza: Methodology, Software, Resources, Investigation, Writing- Reviewing and Editing. Juan C. Vasquez: Formal analysis, Supervision, Writing- Reviewing and Editing. Josep M. Guerrero: Conceptualization, Visualization, Writing- Reviewing and Editing

Declaration of competing interest

The authors declare that they have no known competing financial interests or personal relationships that could have appeared to influence the work reported in this paper.

Acknowledgements

The authors would like to thank the Basque Government's Department of Education for financial support through the Researcher Formation Programme; grant number PRE_2020_2_0038.

The authors would like to thank Fundación Caja Navarra, Obra

Social La Caixa and University of Navarra for financial support through the Mobility Research Formation Programme; grant number MOVIL-2019-25.

J. M. Guerrero was supported by VILLUM FONDEN under the VILLUM Investigator Grant (no. 25920): Center for Research on Microgrids (CROM); www.crom.et.aau.dk.

References

[1] Li J, Lan F, Wei H. A scenario optimal reduction method for wind power time series. IEEE Trans Power Syst 2016;32:1657–8. https://doi.org/10.1109/TPWRS.2015.2412687.
[2] Wüstenhagen R, Bilharz M. Green energy market development in Germany: effective public policy and emerging customer demand. Energy Pol 2006;34:1681–96. https://doi.org/10.1016/j.enpol.2004.07.013.
[3] El-Baz W, Tzscheutschler P, Wagner U. Day-ahead probabilistic PV generation forecast for buildings energy management systems. Sol Energy 2018;171:478–90. https://doi.org/10.1016/j.solener.2018.06.100.
[4] BP. BP energy outlook 2019. 2019. https://www.bp.com/content/dam/bp/business-sites/en/global/corporate/pdfs/energy-economics/energy-outlook/bp-energy-outlook-2019.pdf. [Accessed 4 March 2020].
[5] REN21. Renewables 2019 global satuts report. 2019. https://www.ren21.net/wp-content/uploads/2019/05/gsr_2019_full_report_en.pdf. [Accessed 4 March 2020].
[6] Pillot B, Muselli M, Poggi P, Dias JB. Historical trends in global energy policy and renewable power system issues in Sub-Saharan Africa: the case of solar PV. Energy Pol 2019;127:113–24. https://doi.org/10.1016/j.enpol.2018.11.049.
[7] Maron H, Klemisch H, Maron B. Marktakteure erneuerbare Energie-Anlagen in der Stromerzeugung. 2011. p. 1–92. https://sverigesradio.se/diverse/appdata/isidor/files/3345/12617.pdf. [Accessed 26 July 2020].
[8] Liu J, Fang W, Zhang X, Yang C. An improved photovoltaic power forecasting model with the assistance of aerosol index data. IEEE Transaction on Sustainable Energy 2015;6:434–42. https://doi.org/10.1109/TSTE.2014.2381224.
[9] Li Y, He Y, Su Y, Shu L. Forecasting the daily power output of a grid-connected photovoltaic system based on multivariate adaptive regression splines. Appl Energy 2016;180. https://doi.org/10.1016/j.apenergy.2016.07.052. 392–40.
[10] Ferlito S, Adinolfi G, Graditi G. Comparative analysis of data-driven methods online and offline trained to the forecasting of grid-connected photovoltaic plant production. Appl Energy 2017;205:116–29. https://doi.org/10.1016/j.apenergy.2017.07.124.
[11] Wang Y, Zhang N, Kang C, Miao M, Shi R, Xia Q. An efficient approach to power system uncertainty analysis with high-dimensional dependencies. IEEE Trans Power Syst 2017;33:2984–94. https://doi.org/10.1109/TPWRS.2017.2755698.
[12] Sahoo AK, Sahoo SK. Energy forecasting for grid connected MW range solar PV system. In: 7th India International conference on power electronics (IICPE); 2016. https://doi.org/10.1109/IICPE.2016.8079388.
[13] Yin L, Yu T, Zhang X, Yang B. Relaxed deep learning for real-time economic generation dispatch and control with unified time scale. Energy 2018;149:11–23. https://doi.org/10.1016/j.energy.2018.01.165.
[14] Majumder I, Behera MK, Nayak N. Solar power forecasting using a hybrid EMD-ELM method. In: International conference on circuits power and computing technologies (ICCPCT); 2017. https://doi.org/10.1109/ICCPCT.2017.8074179.
[15] Frías-Paredes L, Mallor F, Gastón-Romeo M, León T. Assessing energy forecasting inaccuracy by simultaneously considering temporal and absolute errors. Energy Convers Manag 2017;142:533–46. https://doi.org/10.1016/j.enconman.2017.03. 056.
[16] Ahmed R, Sreeram V, Mishra Y, Arif MD. A review and evaluation of the state-of-the-art in PV solar power forecasting: techniques and optimization. Renew Sustain Energy Rev 2020;124:109792. https://doi.org/10.1016/j.rser.2020.109792.
[17] Zhang J, Verschae R, Nobuhara S, Lalonde JF. Deep photovoltaic nowcasting. Sol Energy 2018;176:267–76. https://doi.org/10.1016/j.solener.2018.10.024.
[18] Chen X, Du Y, Lim E, Wen H, Jiang L. Sensor network based PV power nowcasting with spatio-temporal preselection for grid-friendly control. Appl Energy 2019;255:113760. https://doi.org/10.1016/j.apenergy.2019.113760.
[19] Chu Y, Li M, Coimbra CFM. Sun-tracking imaging system for intra-hour DNI forecasts. Renew Energy 2016;96:792–9. https://doi.org/10.1016/j.renene.2016.05.041.
[20] Jamal T, Carter C, Schmidt T, Shafiullah GM, Calais M, Urmee T. An energy flow simulation tool for incorporating short-term PV forecasting in a diesel-PV-battery off-grid power supply system. Appl Energy 2019;254:113718. https://doi.org/10.1016/j.apenergy.2019.113718.
[21] Amanpreet K, Nonnenmacher L, Pedro HTC, Coimbra CFM. Benefits of solar forecasting for energy imbalance markets. Renew Energy 2016;86:819–30. https://doi.org/10.1016/j.renene.2015.09.011.
[22] David M, Luis MA, Lauret P. Comparison of intraday probabilistic forecasting of solar irradiance using only endogenous data. Int J Forecast 2018;34:529–47. https://doi.org/10.1016/j.ijforecast.2018.02.003.
[23] Pedro HTC, Coimbra CFM. Assessment of forecasting techniques for solar power production with no exogenous inputs. Sol Energy 2012;86:2017–28. https://doi.org/10.1016/j.solener.2012.04.004.
[24] Sperati S, Alessandrini S, Monache LD. An application of the ECMWF Ensemble Prediction System for short-term solar power forecasting. Sol Energy 2016;113:437–50. https://doi.org/10.1016/j.solener.2016.04.016.
[25] Araya IA, Valle C, Allende H. A Multi-Scale Model based on the Long Short-Term Memory for day ahead hourly wind speed forecasting. Pattern Recogn Lett 2019. https://doi.org/10.1016/j.patrec.2019.10.011.
[26] Verbois H, Rusydi A, Thiery A. Probabilistic forecasting of day-ahead solar irradiance using quantile gradient boosting. Sol Energy 2018;173:313–27. https://doi.org/10.1016/j.solener.2018.07.071.
[27] Gürter M, Paulsen T. The effect of wind and solar power forecasts on day-ahead and intraday electricity prices in Germany. Energy Econ 2018;75:150–62. https://doi.org/10.1016/j.eneco.2018.07.006.
[28] Chazarra M, Pérez-Díaz JI, García-González J, Helseth A. Economic effects of forecasting inaccuracies in the automatic frequency restoration service for the day-ahead energy and reserve scheduling of pumped storage plants. Elec Power Syst Res 2019;174:105850. https://doi.org/10.1016/j.epsr.2019.04.028.
[29] Elsinga B, van Sark WGJHM. Short-term peer-to-peer solar forecasting in a network of photovoltaic systems. Appl Energy 2017;206:1464–83. https://doi.org/10.1016/j.apenergy.2017.09.115.
[30] Lorenz E, Heineman D. Prediction of solar irradiance and photovoltaic power. Compreh Renewable Energy 2012;1:239–92. https://doi.org/10.1016/B978-0-08-087872-0.00114-1.
[31] Diagne M, David M, Lauret P, Boland J, Schmutz N. Review of solar irradiance forecasting methods and a proposition for small-scale insular grids. Renew Sustain Energy Rev 2013;27:65–76. https://doi.org/10.1016/j.rser.2013.06.042.
[32] European Union and International Renewable Energy Agency (IRENA). Renewable energy Prospects for the European union. 2018. https://www.irena.org/-/media/Files/IRENA/Agency/Publication/2018/Feb/IRENA_REmap_EU_2018.pdf. [Accessed 15 July 2020].
[33] International Renewable Energy Agency (IRENA). https://www.irena.org/-/media/Files/IRENA/Agency/Publication/2019/Feb/IRENA_Innovative_ancillary_services_2019.pdf?la=en&hash=F3D83E86922DEED7AA3DE3091F3E49460C9EC1A0. [Accessed 16 July 2020].
[34] Banshwar A, Sharma NK, Sood YR, eta al. Renewable energy sources as a new participant in ancillary service markets. Energy Strategy Reviews 2017;18:106–20. https://doi.org/10.1016/j.esr.2017.09.009.
[35] Ayvazoğluyüksel Ö, Filik ÜB. Estimation methods of global solar irradiation, cell temperature and solar power forecasting: a review and a case study in Eskişehir. Renew Sustain Energy Rev 2018;91:639–53. https://doi.org/10.1016/j.rser.2018.03.084.
[36] Rodríguez F, Bazmohammadi N, Guerrero JM, Galarza A. A very short-term probabilistic prediction interval forecaster for reducing load uncertainty level in smart grids. Appl Sci 2021;11(6):2538. https://doi.org/10.3390/app11062538.
[37] Rodríguez F, Genn M, Fontán L, Galarza A. Very short-term temperature forecaster using MLP and N-nearest stations for calculating key control parameters in solar photovoltaic generation. Sustainable Energy Technologies and Assessments 2021;45:101085. https://doi.org/10.1016/j.seta.2021.101085.
[38] Rodríguez F, Florez-Tapia AM, Fontán L, Galarza A. Very short-term wind power density forecasting trough artificial neural networks for microgrid control. Renew Energy 2020;145:1517–27. https://doi.org/10.1016/j.renene.2019.07.067.
[39] Dupré A, Dobrinski P, Alnzo B, Bados J, Briad C, Plougoven R. Sub-hourly forecasting of wind speed and wind energy. Renew Energy 2020:2373–9. https://doi.org/10.1016/j.renene.2019.07.161.
[40] Wang GC, Urquhart B, Kleissl J. Cloud base height estimates from sky imagery and a network of pyranometers. Sol Energy 2019;184:594–609. https://doi.org/10.1016/j.solener.2019.03.101.
[41] Polo J. Solar global horizontal and direct normal irradiation maps in Spain derived from geostationary satellites. J Atmos Sol Terr Phys 2015;130–131:81–8. https://doi.org/10.1016/j.jastp.2015.05.015.
[42] Agoua XG, Girard R, Kariniotakis G. Short-term spatio-temporal forecasting of photovoltaic power production. IEEE Transactions on Sustainable Energy 2018;9:538–46. https://doi.org/10.1109/TSTE.2017.2747765.
[43] Tang N, Mao S, Wang Y, Nelms RM. Solar power generation forecasting with a LASSO- based approach. IEEE Internet of Things Journal 2018;5:2933–44. https://doi.org/10.1109/JIOT.2018.2877510.
[44] Prado F, Minutolo MC, Kristjanpoller W. Forecasting based on an ensemble autoregressive moving average - adaptive neuro - fuzzy inference system – neural network - genetic algorithm framework. Energy 2020;197:117159. https://doi.org/10.1016/j.energy.2020.117159.
[45] David M, Ramahatana F, Trombe PJ, Lauret P. Probabilistic forecasting of the solar irradiance with recursive ARMA and GARCH models. Sol Energy 2016;133:55–72. https://doi.org/10.1016/j.solener.2016.03.064.
[46] Singh ASN, Mohapatra A. Repeated wavelet transform based ARIMA model for very short-term wind speed forecasting. Renew Energy 2019;136:758–68. https://doi.org/10.1016/j.renene.2019.01.031.
[47] Rodríguez F, Fleetwood A, Galarza A, Fontán F. Predicting solar energy generation through artificial neural networks using weather forecasts for microgrid control. Renew Energy 2018;126:855–64. https://doi.org/10.1016/j.renene.2018.03.070.
[48] Jahangir H, Golkar MA, Alhameli F, Mazouz A, Ahmadian A, Elkamel A. Short-

term wind speed forecasting framework based on stacked denoising auto-encoders with rough ANN. Sustain. Energy Technol. Assess. 2020;38:100601. https://doi.org/10.1016/j.seta.2019.100601.
[49] Rodríguez F, Martín F, Fontán L, Galarza A. Very short-term load forecaster based on a neural network technique for smart grid control. Energies 2020;13(19):5210. https://doi.org/10.3390/en13195210.
[50] Lv X, Duan F, Jiang JJ, Fu X, Gan L. Deep metallic surface defect detection: the new benchmark and detection network. Sensors 2020;20:1562. https://doi.org/10.3390/s20061562.
[51] Sharma V, Yang D, Walsh W, Reindl T. Short term solar irradiance forecasting using a mixed wavelet neural network. Renew Energy 2016;90:481–92. https://doi.org/10.1016/j.renene.2016.01.020.
[52] Cheng Y, Zhang S, Zhang W, Peng J, Cai Y. Multi-factor spatio-temporal correlation model based on a combination of convolutional neural network and long short-term memory neural network for wind speed forecasting. Energy Convers Manag 2019;185:783–99. https://doi.org/10.1016/j.enconman.2019.02.018.
[53] Li K, Wang R, Lei H, Zhang T, Liu Y, Zheng X. Interval prediction of solar power using an improved bootstrap method. Sol Energy 2018;159:97–112. https://doi.org/10.1016/j.solener.2017.10.051.
[54] Liu L, Zhao Y, Chang D, Xie J, Ma Z, Sun Q, Yin H, Wennerten R. Prediction of short-term PV power output and uncertainty analysis. Appl Energy 2018;228:700–11. https://doi.org/10.1016/j.apenergy.2018.06.112.
[55] Liu Y, Qin H, Zhang Z, Pei S, Jiang Z, Feng Z, Zhou J. Probabilistic spatiotemporal wind speed forecasting based on a variational Bayesian deep learning model. Appl Energy 2020;260:114259. https://doi.org/10.1016/j.apenergy.2019.114259.
[56] Wan C, Lin J, Song Y, Xu Z, Yang G. Probabilistic forecasting of photovoltaic generation: an efficient statistical approach. IEEE Trans Power Syst 2017;32:2741–2. https://doi.org/10.1109/TPWRS.2016.2608740.
[57] Chu Y, Li M, Pedro HTC, Coimbra CFM. Real-time prediction intervals for intra-hour DNI forecasts. Renew Energy 2015;83:234–44. https://doi.org/10.1016/j.renene.2015.04.022.
[58] Zhang J, Yan J, Infield D, Liu Y, Lien F. Short-term forecasting and uncertainty analysis of wind turbine power based on log sort-term memory network and Gaussian mixture model. Appl Energy 2019;241:229–44. https://doi.org/10.1016/j.apenergy.2019.03.044.
[59] Junior JGDSF, Oozeki T, Ohtake H, Takashima T, Ogimoto K. On the use of maximum likelihood and input data similarity to obtain prediction intervals for forecasts of photovoltaic power generation. Journal of Electrical Engineering and Technology 2015;10:1342–8. https://doi.org/10.5370/JEET.2015.10.3.1342.
[60] Khosravi F, Izbirak G, Shavarani SM. Application of bootstrap re-sampling method in statistical measurement of sustainability. Soc Econ Plann Sci 2020. https://doi.org/10.1016/j.seps.2020.100781. XXXXXXX.
[61] Yan J, Liu Y, Han S, Wang Y, Feng S. Rewievs on uncertainty analysis of wind power forecasting. Renew Sustain Energy Rev 2015;52:1322–30. https://doi.org/10.1016/j.rser.2015.07.197.
[62] Rodríguez F, Martín F, Fontán L, Galarza A. Ensemble of machine learning and spatiotemporal parameters to forecast very short-term solar irradiation to compute photovoltaic generators' output power. Energy 2021;229:120647. https://doi.org/10.1016/j.energy.2021.120647.
[63] Marquardt DW. An algorithm for least-squares estimation of nonlinear parameters. SIAM J Appl Math 1963;11(2):431–41. https://doi.org/10.1137/0111030.
[64] Seber GA, Wild CJ. Nonlinear regression. New York: John Wiley & Sons, Inc.; 1989. https://doi.org/10.1002/0471725315.
[65] Yan X, Abbes D, Francois B. Uncertainty analysis for day ahead power reserve quantification in an urban microgrid including PV generators. Renew Energy 2017;106:288–97. https://doi.org/10.1016/j.renene.2017.01.022.
[66] Ni Q, Zhuang S, Sheng H, Kang G, Xiao J. An ensemble prediction intervals approach for short-term PV power forecasting. Sol Energy 2017;155:1072–83. https://doi.org/10.1016/j.solener.2017.07.052.
[67] Pedro HTC, Coimbra CFM, David M, Lauret P. Assessment of machine learning techniques for deterministic and probabilistic intra-hour solar forecasts. Renew Energy 2018;123:191–203. https://doi.org/10.1016/j.renene.2018.02.006.